# Photoelastic and elastic properties of the fluorite structure materials, LiF, and Si

Zachary H. Levine, John H. Burnett, and Eric L. Shirley
*National Institute of Standards and Technology, Gaithersburg, Maryland 20899, USA*
(Received 25 June 2003; published 28 October 2003)

We present computational results of the photoelastic and elastic properties of $CaF_2$, $SrF_2$, $BaF_2$, $Ca_xSr_{1-x}F_2$, $x=0.25,0.50,0.75$, LiF, and Si. We also present measurements of the photoelastic properties in the visible through the ultraviolet of $CaF_2$, $SrF_2$, and $BaF_2$. At least semiquantitative agreement is obtained with most experimental results for all properties, including the low-frequency behavior and dispersion of the photoelastic tensor components.

DOI: 10.1103/PhysRevB.68.155120 PACS number(s): 78.20.Bh, 78.20.Fm, 71.15.Nc

## I. INTRODUCTION

The feature sizes in integrated circuits have been reduced by orders of magnitude over the past decades, from 25 $\mu$m in 1965 (Ref. 1) to an estimated 0.1 $\mu$m in 2003 (Ref. 2). As part of this transition, the wavelengths of light used to expose the circuits have been reduced from the visible into the ultraviolet ($\leqslant$400 nm) and vacuum ultraviolet (VUV, $\leqslant$200 nm). Planned transitions from the use of light at 248–193 nm and, later, 157 nm require that fused silica, used for photolithography, be abandoned in favor of materials with higher band gaps, of which calcium fluoride is the principal candidate.

The optics of photolithography steppers must be precisely characterized. Small deviations in the index of refraction may lead to a degradation in the quality of the focus, which in turn may prevent the features from being defined as precisely as required. In previous works, we investigated one of the sources of such deviation, intrinsic birefringence, due to the finite wavelength of light, discussing the magnitude of the effect,[3] its symmetry, and implications for VUV optics.[4]

Another key issue for photolithography is birefringence induced by stress or strain (i.e., photoelasticity) in, specifically, $CaF_2$.[5] In this paper, we present measurements of the photoelastic constants of $CaF_2$ and the alternate VUV materials $SrF_2$ and $BaF_2$ from the visible into the VUV. Additionally, we present calculations of the elastic and photoelastic constants of $CaF_2$, $SrF_2$, $BaF_2$, and LiF. Because $CaF_2$ and $SrF_2$ have alternate signs for their intrinsic birefringence at 157 nm (Ref. 3) and solid solutions $Ca_xSr_{1-x}F_2$ are known to exist,[6,7] we proposed the use of the mixed crystal with $x \approx 0.33$, because the intrinsic birefringence would be nearly zero.[8] We present a theoretical determination of the elastic and photoelastic properties of these mixed crystals.

Calculations for silicon are also presented to make contact with the existing literature on elastic and photoelastic properties. In particular, a comparison of the internal strain parameter $\zeta$ to experiment and to an earlier generation of density-functional-based calculations is possible for silicon, but not for any of the fluoride materials we considered. The predicted value of the photoelastic constants is sensitive to the internal strain parameter.

## II. TENSORS: MATHEMATICAL AND COMPUTATIONAL ASPECTS

Several photoelastic tensors have been defined in the literature. Here we consider the change in the dielectric constant $\delta\epsilon_{ij}$ with respect to a strain $\eta_{k\ell}$:

$$\delta\epsilon_{ij} = \sum_{k\ell} K_{ijk\ell}\eta_{k\ell}. \tag{1}$$

Here $i$, $j$, $k$, and $\ell$ are Cartesian indices, and the photoelastic tensor $K_{ijk\ell}$ is implicitly defined. The relationship

$$\sigma_{ij} = \sum_{k\ell} C_{ijk\ell}\eta_{k\ell} \tag{2}$$

relates stress $\sigma_{ij}$ to strain, where the $C_{ijk\ell}$ are the elastic moduli. Experimentally, the stress is typically the independent variable, but stress may converted to strain using the elastic moduli. In this paper, such conversions are performed using experimental values for the elastic moduli.[9–13] Both $\delta\epsilon_{ij}$ and $\sigma_{ij}$ are symmetric in the permutation of the indices. Given that $K$ and $C$ must respect the same cubic point group, they are simultaneously diagonalizable.[14] For the cubic crystals with fourfold axes, including all those considered in this work, these eigenvalues are $K_{11}+2K_{12}$, $K_{11}-K_{12}$, and $K_{44}$, with similar expressions for $C$. [We adopt the convention that pairs of indices are compressed according the Voight rule $(11,22,33,23,31,12)\rightarrow(1,2,3,4,5,6)$, but all symbols with compressed subscripts are equal to their uncompressed counterparts, e.g., $K_{44}\equiv K_{2323}$.] The eigenvectors of strain are hydrostatic compression, compression along an (001) direction, and compression along a (111) direction. In the case of the diamond and fluorite structures, only the (111) compression permits a single internal strain parameter.

We performed the calculation of the three components of $K$ using finite differences. The optical-constant equations (described in the next section) were evaluated for several electric field polarizations $\hat{E}$ and several strains $\eta_{k\ell}$. The calculation was performed with the wave vector of light $\vec{q}=0$. The program produced the quantity $\Sigma_{ij}E_iE_j\epsilon_{ij}$. The calculation was performed for $\hat{E}\propto[110]$, $[101]$, $[011]$, $[1\bar{1}0]$, $[10\bar{1}]$, and $[0\bar{1}1]$. (It was not necessary to repeat most of the calculation when $\hat{E}$ was varied.) These six val-

ues of the polarization produced the six linear combinations $\frac{1}{4}\epsilon_{ii} \pm \frac{1}{2}\epsilon_{ij} + \frac{1}{4}\epsilon_{jj}$ of the components of the real symmetric dielectric tensor for $i \neq j$. From these six values, the six components of the symmetric tensor $\epsilon_{ij}$ were found. Although cubic symmetry could have been exploited to reduce the amount of calculation somewhat, the method chosen here averages over small, artificial symmetry breaking remaining in the code and is general.

The calculation was performed for several strains, each yielding the dielectric function $\epsilon_{ij}(\omega; \eta_{k\ell})$. The strain was obtained using the relation[15]

$$a'_{ij} = \sum_k (\delta_{ik} + \eta_{ik}) a_{kj}, \tag{3}$$

where for each $j = 1,2,3$, $a_{kj}$ are the three components of the direct lattice vector of the unstrained lattice, with $a'_{ij}$ the corresponding quantities for the strained lattice; $\delta_{ik}$ is the Kronecker delta. For each strain type, $\delta\epsilon_{ij}$ was obtained using finite differences from six magnitudes for LiF and $CaF_2$ ($\pm 0.01\%$, $\pm 0.02\%$, and $\pm 0.03\%$) and four magnitudes ($\pm 0.01\%$ and $\pm 0.02\%$) for the other materials. These strains are taken about the experimental lattice constant. The differences between four-point and six-point derivatives were negligible for strains of order 0.1%. The elastic moduli were determined by obtaining the quadratic term from a fit of total energies using typically 14 uniformly spaced strains per direction over $\pm 26\%$, about the experimental lattice constant. (In some cases, some of the larger distortions resulted in metallization of the crystal and such values were omitted. As an extreme case, 16 values over the range from $-18\%$ to $+12\%$ were used for silicon.) Larger distortions were necessary for the elastic moduli than for the photoelastic tensor because the total energy has a quadratic minimum at the theoretical lattice constant. To obtain the elastic moduli, the second derivative was evaluated at the theoretical lattice constant, which differed by a couple of percent from the experimental value, as detailed in Table I.

In most cases, three strain types were chosen: namely, hydrostatic, uniaxial (001), and uniaxial (111) strain. However, for the case of LiF, the absence of an internal strain parameter permitted the calculation to be simplified to just two strain types—hydrostatic and uniaxial (110)—with two components of $\delta\epsilon$ obtained at once with the (110) strain.

TABLE I. Parameters used in the calculation. The experimental lattice constants are given. The energy cut off for the plane-wave expansion set, $E_{\text{cut}}$, used in both for the LDA calculation and to solve the Bethe-Salpeter equation, is given. The number of $k$ points $N_k$ in the full Brillouin zone for each (equivalent) dimension is given. For the undistorted cubic crystals, $2\times2\times2$, $4\times4\times4$, $6\times6\times6$, $8\times8\times8$, $10\times10\times10$, and $12\times12\times12$ in the full Brillouin zone correspond to 2, 10, 28, 60, 110, and 182 special points in the irreducible Brillouin zone (Ref. 57). In the case of the mixed crystals, the ''experimental'' lattice constant is obtained by Vegard's law (Ref. 58).

| | Expt. lattice constant (pm) | LDA lattice constant (pm) | $E_{\text{cut}}$ (Ry) | $N_k$ |
|---|---|---|---|---|
| Si | 542.9 | 536.2 | 20 | 4 |
| LiF | 402.0 | 394.0 | 100 | 4 |
| $CaF_2$ | 546.4 | 531.0 | 100 | 4 |
| $Ca_{0.75}Sr_{0.25}F_2$ | 556.2 | 542.3 | 100 | 4 |
| $Ca_{0.50}Sr_{0.50}F_2$ | 565.0 | 551.8 | 100 | 4 |
| $Ca_{0.25}Sr_{0.75}F_2$ | 572.7 | 559.9 | 100 | 4 |
| $SrF_2$ | 579.6 | 566.6 | 100 | 4 |
| $BaF_2$ | 619.6 | 592.9 | 100 | 4 |

## III. THEORY AND COMPUTATION OF THE LIGHT-MATTER INTERACTION

Calculations were carried out within the pseudopotential and plane-wave framework. Pseudopotentials were constructed using the Hamann-Schlüter-Chiang approach[16] using cutoff functions of Vanderbilt[17] for enhanced smoothness. For structural calculations, pseudopotentials in the local-density approximation (LDA) were used. For optical calculations, Hartree-Fock pseudopotentials enhanced by core-polarization potentials[18] were used. Similarly, although we determined the elastic moduli about the theoretical lattice constant, we used the experimental lattice constants for optical properties, because these give better results for photoelastic[14] and other optical constants.[19] Throughout this work, Ceperley-Alder correlation was used[20] as parametrized by Perdew and Zunger.[21] Pseudopotential nonlocality was treated using multiple projectors as described elsewhere.[22] The same reference also describes the iterative diagonalization techniques used.

For optical calculations, we used the approach of Benedict and Shirley.[23] This approach is based on the Bethe-Salpeter equation, and much of its justification is discussed by Benedict and Shirley.[23] It assumes that a single Slater determinant can describe the ground-state wave function and that optically excited states can be described as linear superpositions of states formed by promoting an electron from an occupied band to an unoccupied band, producing an electron-hole pair. We may denote the ground state as $|0\rangle$ and define its energy to be zero for purposes of optical calculations. A generic electron promotion would excite an electron in band $n$ at wave vector $\mathbf{k}$ to a different band $n'$. The resulting state, which is not a stationary state, may be denoted as $|nn'\mathbf{k}\rangle$. The states $\{|nn'\mathbf{k}\rangle\}$ are assumed to form an orthonormal basis for optically excited states.

The excited-state Hamiltonian may be written as $H = H_e + H_h + V_D + V_X$. Here $H_e$ and $H_h$ account for the electron and hole energy, and are diagonal in the $\{|nn'\mathbf{k}\rangle\}$ basis. One has $(H_e + H_h)|nn'\mathbf{k}\rangle = (E_{n'\mathbf{k}} - E_{n\mathbf{k}})|nn'\mathbf{k}\rangle$, where $E_{n\mathbf{k}}$ denotes a quasiparticle band energy that is approximated as an LDA Kohn-Sham eigenvalue with a scissor-type correction to the band gap[24] and a 17% enhancement of the valence bandwidth in fluorides. Such corrections to the band structure were explicitly calculated in Si,[22] LiF, and $CaF_2$,[25] and borrowed from $CaF_2$ for other alkaline-earth fluorides and alloys. $V_D$ and $V_X$ account for the direct and exchange parts of the electron-hole interaction, respectively. We may denote the Bloch function at wave vector $\mathbf{k}$ in band $n$ by $\psi_{n\mathbf{k}}(\mathbf{r})$ and so forth. We then have

$$\langle n''n'''\mathbf{k}'|V_D|nn'\mathbf{k}\rangle = -\int d^3\mathbf{r}_e \int d^3\mathbf{r}_h W(\mathbf{r}_e,\mathbf{r}_h) \times \psi^*_{n'''\mathbf{k}'}(\mathbf{r}_e)\psi_{n'\mathbf{k}}(\mathbf{r}_e)\psi^*_{n\mathbf{k}}(\mathbf{r}_h)\psi_{n''\mathbf{k}'}(\mathbf{r}_h) \tag{4}$$

and

$$\langle n''n'''\mathbf{k}'|V_X|nn'\mathbf{k}\rangle = 2\int d^3\mathbf{r}\int d^3\mathbf{r}'\,\overline{v}(\mathbf{r},\mathbf{r}') \times \psi^*_{n'''\mathbf{k}'}(\mathbf{r}')\psi_{n''\mathbf{k}'}(\mathbf{r}')\psi^*_{n\mathbf{k}}(\mathbf{r})\psi_{n'\mathbf{k}}(\mathbf{r}). \tag{5}$$

Here $\overline{v}$ is the bare Coulomb interaction excluding the macroscopic component (i.e., excluding the [000] reciprocal lattice vector), $W$ is the statically screened Coulomb interaction, and the factor of 2 is for the spin degeneracy. $W$ was computed using the Levine-Louie[26] model with local-field effects included according to Hybertsen and Louie.[27] The experimental value for the static dielectric function was used.

An element of the dielectric tensor, $\epsilon_{ij}(\omega)$ for frequency $\omega$, was deduced from the appropriate expression for $\mathrm{Im}\,\epsilon_{ij}(\omega>0)$:

$$\mathrm{Im}\,\epsilon_{ij}(\omega>0) = -\frac{4\pi}{\omega^2}\,\mathrm{Im}\langle 0|J_i\frac{1}{\omega-H+i\eta}J_j|0\rangle, \tag{6}$$

where $J$ is the current operator and $i\eta$ is a positive imaginary infinitesimal. As written, the expression is appropriate. However, we evaluated a current matrix element using one-electron matrix elements with LDA wave functions. This amounts to the formal replacement

$$\omega^{-1}\langle nn'\mathbf{k}|J_j|0\rangle \rightarrow (E^{\mathrm{LDA}}_{n'\mathbf{k}}-E^{\mathrm{LDA}}_{n\mathbf{k}})^{-1}\langle\psi_{n'\mathbf{k}}|J_j|\psi_{n\mathbf{k}}\rangle. \tag{7}$$

This cancels the $\omega^{-2}$ factor in the expression for $\mathrm{Im}\,\epsilon_{ij}(\omega>0)$. Such a substitution appears to be standard in current Bethe-Salpeter work, and it does not appear to constitute a significant approximation.

Following evaluation of $\mathrm{Im}\,\epsilon_{ij}(\omega>0)$ by the Haydock recursion method, as detailed by Benedict and Shirley,[23] one may extend the result to $\omega<0$ using time-reversal symmetry and obtain $\mathrm{Re}\,\epsilon_{ij}(\omega)$ by Kramers-Kronig analysis. In practice, these steps are all done at once in the Haydock recursion method.

## IV. EXPERIMENTAL METHOD

The photoelastic constants $K_{11}-K_{12}$ and $K_{44}$ were determined for $CaF_2$, $SrF_2$, and $BaF_2$ for wavelengths from the visible down to 156 nm in the vacuum ultraviolet, from piezobirefringence measurements. Procedures used were similar to those described by Feldman[28] modified to operate in the vacuum ultraviolet. To determine the constant $K_{11}-K_{12}$, for each material a rectangular prism was prepared with dimensions 30 mm×12 mm×12 mm, with polished faces normal to the crystallographic directions [001], [110], $[\bar{1}10]$, respectively. Uniaxial stress was applied along the long (i.e., [001]) direction. To determine the constant $K_{44}$, for each material a rectangular prism was prepared with dimensions 30 mm×12 mm×12 mm, with polished faces normal to the crystallographic directions [111], $[\bar{1}10]$, $[11\bar{2}]$, respectively. Uniaxial stress was applied along the long (now, [111]) direction. Orientations were determined by back-reflection Laue measurements to within 2°.

The uniaxial stressing apparatus used is discussed in Ref. 29. The sample ends were placed in brass cups, with indium foil between the sample and the cups to ensure uniformity of the stress across the contact surfaces. The stress was applied continuously by a clamp, driven by a lever arm adjusted by a fine-pitched screw. The stress values were determined by a piezotransducer calibrated by weights. The sample in the stressing apparatus was mounted between crossed $MgF_2$ Rochon linear polarizers, with the stress axis 45° to the polarizer axes. Collimated monochromatic light from atomic spectral lines from various spectral line sources was sent through the polarizers and sample. As birefringence was induced in the sample by the applied stress, a phase difference was generated between the light components parallel and perpendicular to the stress direction, given by

$$\delta = \frac{2\pi t}{\lambda}(n_\parallel - n_\perp), \tag{8}$$

where $t$ is the thickness of the material, and $n_\parallel$ and $n_\perp$ are the indices of refraction of the material at that wavelength parallel and perpendicular to the stress direction. This phase shift resulted in elliptically polarized light partially transmitted through the second linear polarizer. The magnitude and sign of the phase shift were determined by the amount of compensating phase shift needed by a $MgF_2$ Soleil-Babinet compensator, placed between the crossed polarizers, to null out the signal. The entire apparatus was operated in a nitrogen gas purge tent to allow measurements for wavelengths in the vacuum ultraviolet.

For each material, for each of the two crystal orientations, and for each wavelength, measurements of the phase shift were made for a series of stress values. Let $Q^{(n)}_{[001]}$ be the linear coefficient relating differences of the index to uniaxial stress applied along the [001] direction, i.e.,

$$[n_\parallel - n_\perp]_{[001]} = Q^{(n)}_{[001]}\sigma \quad \text{for stress along } [001]. \tag{9}$$

Similarly, let $Q^{(n)}_{[111]}$ be defined as

$$[n_\parallel - n_\perp]_{[111]} = Q^{(n)}_{[111]}\sigma \quad \text{for stress along } [111]. \tag{10}$$

Relating stress to strain by the measured elastic constants $C_{11}-C_{12}$ and $C_{44}$ given in Table II and using the relation $\epsilon_\parallel-\epsilon_\perp \approx 2n_0(n_\parallel-n_\perp)$ with the unstressed indices $n_0$ from the literature, the photoelastic constants were determined by

$$[\epsilon_\parallel - \epsilon_\perp]_{[001]} = (K_{11}-K_{12})\eta_3 \quad \text{for strain along } [001] \tag{11}$$

and

$$[\epsilon_\parallel - \epsilon_\perp]_{[111]} = K_{44}\eta_4 \quad \text{for strain along } [111], \tag{12}$$

TABLE II. Elastic moduli for silicon, LiF, and fluorite-structure compounds in GPa. The bulk modulus is $B=\frac{1}{3}(C_{11}+2C_{12})$. The linear combinations shown correspond to hydrostatic strain and uniaxial strain along the [001] and [111] directions, respectively.

| | | | $C_{11}+2C_{12}$ | $C_{11}-C_{12}$ | $C_{44}$ | |
|---|---|---|---|---|---|---|
| Si | LDA | Ref. 30 | 281 | 98 | 85 | |
| | LDA | Ref. 31 | 291 | 99 | 78.5 | |
| | LDA | Present | 294.81 | 100.94 | 81.18 | |
| | Expt. | Ref. 9 | 297.4 | 102.5 | 80.07 | 73 K |
| LiF | LDA | Ref. 33 | 212 | | | |
| | LDA | Present | 220 | 70 | 58.3 | |
| | Expt. | Ref. 10 | 209.4 | 82.2 | 64.9 | 4.2 K |
| $CaF_2$ | LDA | Ref. 34 | 310.5 | 129.1 | 49.2 | |
| | LDA | Present | 305 | 122 | 34.0 | |
| | Expt. | Ref. 11 | 264.54 | 124.02 | 36.08 | 77.35 K |
| | Expt. | Ref. 11 | 254.09 | 120.56 | 33.83 | 295.5 K |
| $Ca_{0.75}Sr_{0.25}F_2$ | LDA | Present | 297 | 110 | 35.0 | |
| $Ca_{0.50}Sr_{0.50}F_2$ | LDA | Present | 276 | 98 | 33.0 | |
| $Ca_{0.25}Sr_{0.75}F_2$ | LDA | Present | 257 | 88 | 32.4 | |
| $SrF_2$ | LDA | Ref. 34 | 248.1 | 86.1 | 30.3 | |
| | LDA | Present | 243 | 81 | 31.6 | |
| | Expt. | Ref. 13 | 223.8 | 81.3 | 33.08 | Extrapolated to 0 K |
| | Expt. | Ref. 13 | 209.6 | 80.4 | 31.28 | 300 K |
| $BaF_2$ | LDA | Ref. 34 | 223.2 | 52.2 | 20.14 | |
| | LDA | Present | 219 | 56 | 27.4 | |
| | Expt. | Ref. 12 | 187.72 | 53.29 | 25.44 | Extrapolated to 0 K |
| | Expt. | Ref. 12 | 169.2 | 49.13 | 25.35 | 300 K |

where $\eta_3$ and $\eta_4$ are the uniaxial strains along the respective directions.

The results of the experiment are given in Table III and several of the figures.

## V. STRUCTURAL PROPERTIES

Our main interest in this paper is the photoelastic properties of the fluorides. For [111] strains, it is necessary to consider the internal strain parameter $\zeta$, which characterizes the single internal degree of freedom of the atoms whose bonds are directed along [111] compared to the (still equivalent) $[\bar{1}11]$, $[1\bar{1}1]$, and $[11\bar{1}]$ directions. We are not aware of any measurements of $\zeta$ for the fluorides. As such data do exist for silicon, silicon is included in the study. In the case of silicon, the photoelastic properties of silicon are known to be strongly dependent on $\zeta$ (Ref. 14).

### A. Elastic moduli

The elastic constants of silicon have been predicted well by density-functional theory for some time.[30,31] As seen in Table II, our calculation is in good agreement with the previous calculations and experiment for all three independent tensor components.

The elastic moduli for fluorite-structure materials $CaF_2$, $SrF_2$, $Ca_xSr_{1-x}F_2$, and $BaF_2$, as well as LiF, are also shown in Table II. The agreement with experiment is at the 10% level, compared to 1% for silicon. The series from Ca to Sr to Ba obeys a trend of softening, as one would guess from the increasing atomic radius of the cation. The alloys, studied here in the virtual-crystal approximation, largely obey this trend, but there is a small exception for $C_{44}$ for $Ca_{0.75}Sr_{0.25}F_2$. The agreement with experiment tends to improve when the comparison is made with 0 K data. (A review of static and dynamic properties of fluorite-structure materials[32] was helpful in preparing Table II.)

Table II also presents other local-density-functional calculations of the elastic moduli of the fluorides.[33,34] The elastic moduli calculations of Mérawa *et al.*[34] also include the Hartree-Fock, generalized gradient approximation, and a hybrid functional due to Becke.[35] Mérawa *et al.* concluded that the more advanced methods were better than the LDA. Our calculations support this interpretation for the bulk modulus: however, for the other elastic moduli (i.e., $C_{11}-C_{12}$ and $C_{44}$) we find the LDA to be highly satisfactory. In particular, our values for $C_{44}$ for $CaF_2$ and $BaF_2$ differ significantly from the calculation of Mérawa *et al.*, which overestimated the experimental trend in this isoelectronic series. Perhaps the principal difference between our methods is the use of the pseudopotential and plane-wave approximation in our calculation versus the use of an atomic orbital basis set by Mérawa *et al.*

### B. Internal strain parameter $\zeta$

When silicon, a diamond-structure material, is compressed in the [111] direction, the [111] bonds between the

TABLE III. Experimental results. The photoelastic constants for various fluorite-structure materials, measured at a series of photon energies. The values of $Q^{(n)}_{[001]}$ and $Q^{(n)}_{[111]}$ are measured for stress applied in the [001] and [111] directions, respectively. The values for $K_{11}-K_{12}$ and $K_{44}$ are derived from the $Q^{(n)}$, the indices of refraction, and the room-temperature elastic moduli given in Table II using several equations presented in the text. The unstressed index of refraction is denoted by $n_0$. One standard total uncertainty is given in parentheses. The principal contribution to the uncertainty comes from the relative phase measurements, evaluated from a statistical analysis of repeated independent measurements.

| | Photon energy (eV) | $n_0$ | $Q^{(n)}_{[001]}$ ($TPa^{-1}$) | $Q^{(n)}_{[111]}$ ($TPa^{-1}$) | $K_{11}-K_{12}$ | $K_{44}$ |
|---|---|---|---|---|---|---|
| $CaF_2$ | 2.269 | 1.435[a] | 2.25(2) | −1.10(2) | 0.780(8) | −0.107(2) |
| | 2.844 | 1.439[a] | 2.31(2) | −1.10(2) | 0.801(8) | −0.107(2) |
| | 3.396 | 1.445[a] | 2.36(2) | −1.11(2) | 0.823(8) | −0.109(2) |
| | 4.886 | 1.466[a] | 2.62(3) | −1.16(2) | 0.925(9) | −0.115(2) |
| | 6.421 | 1.502[b] | 3.01(3) | −1.11(2) | 1.090(10) | −0.113(2) |
| | 7.943 | 1.563[c] | 3.65(4) | −0.87(2) | 1.375(14) | −0.092(2) |
| $SrF_2$ | 2.269 | 1.439[d] | 3.19(2) | −0.907(4) | 0.737(4) | −0.0817(5) |
| | 2.844 | 1.444[d] | 3.25(2) | −0.913(4) | 0.754(4) | −0.0824(5) |
| | 3.396 | 1.450[d] | 3.36(2) | −0.922(4) | 0.784(4) | −0.0836(5) |
| | 4.886 | 1.472[d] | 3.73(2) | −0.961(4) | 0.882(4) | −0.0885(5) |
| | 6.421 | 1.512[d] | 4.30(2) | −0.996(4) | 1.044(4) | −0.0942(5) |
| | 7.943 | 1.576[c] | 5.07(4) | −1.034(8) | 1.283(8) | −0.1020(10) |
| $BaF_2$ | 2.269 | 1.476[d] | 4.99(5) | −1.59(3) | 0.723(7) | −0.119(2) |
| | 2.844 | 1.482[d] | 5.13(5) | −1.64(3) | 0.747(7) | −0.123(2) |
| | 3.396 | 1.489[d] | 5.29(5) | −1.66(3) | 0.774(8) | −0.125(2) |
| | 4.886 | 1.518[d] | 6.01(6) | −1.82(4) | 0.897(9) | −0.140(2) |
| | 6.421 | 1.584[b] | 7.38(7) | −2.15(4) | 1.149(11) | −0.172(2) |
| | 7.943 | 1.664[c] | 10.2(1) | −2.93(6) | 1.664(17) | −0.235(3) |

[a]Reference 59.
[b]Reference 60.
[c]Reference 61.
[d]Reference 62.

two silicon atoms become inequivalent to those in the $[\bar{1}11]$, $[1\bar{1}1]$, and $[11\bar{1}]$ directions. The bond length along [111] is determined not by symmetry, but by energy minimization. However, even under strain there is a threefold rotational symmetry. The $[\bar{1}11]$, $[1\bar{1}1]$, and $[11\bar{1}]$ bonds remain equivalent to each other, and the direction of the [111] bond is not free. This single degree of freedom is usually characterized by the parameter $\zeta$, introduced by Kleinman.[36] When $\zeta=0$, the silicon atoms are displaced proportionately to the macroscopic strain. When $\zeta=1$, the bond lengths of the four bonds about a given silicon atom remain equal to each other, although not to the bond length in the undistorted crystal; moreover, their bond angles change to follow the tetragonal distortion. The atomic coordinates vary linearly with $\zeta$. The condition $\zeta=1$ would occur with central forces; physical angular forces require $0<\zeta<1$ (Ref. 36). Under hydrostatic strain or $[1\bar{1}0]$ strain there are no internal degrees of freedom.

TABLE IV. Internal strain parameter $\zeta$, a pure number, for silicon, LiF, and fluorite-structure compounds. If an entry is given for $\zeta'$, that value was reported in its reference as $\zeta$ (but $\Omega$ for the fluorides) and is multiplied by 1.5 to convert to $\zeta$.

| | | | $\zeta$ | $\zeta'$ |
|---|---|---|---|---|
| Si | Expt. | Ref. 63 | 0.75±0.07 | |
| | Expt. | Ref. 64 | 0.65±0.04 | |
| | Expt. | Ref. 45 | 0.72±0.04 | |
| | Expt. | Ref. 46 | 0.74±0.04 | |
| | LDA | Ref. 30 | 0.795 | 0.53 |
| | LDA | Ref. 31 | 0.82 | 0.545 |
| | LDA | Present | 0.81 | |
| $CaF_2$ | LDA | Present | 0.47 | |
| | Force field | Ref. 40 | 0.324 | 0.216 |
| $Ca_{0.75}Sr_{0.25}F_2$ | LDA | Present | 0.53 | |
| $Ca_{0.50}Sr_{0.50}F_2$ | LDA | Present | 0.57 | |
| $Ca_{0.25}Sr_{0.75}F_2$ | LDA | Present | 0.60 | |
| $SrF_2$ | LDA | Present | 0.62 | |
| | Force field | Ref. 40 | 0.399 | 0.266 |
| $BaF_2$ | LDA | Present | 0.67 | |
| | Force field | Ref. 40 | 0.566 | 0.377 |

There are at least four reported measurements of the internal strain parameter, which are summarized in Table IV. Models of the internal strain parameter have been summarized by Cousins.[37] Here we restrict our attention to calculations performed using density-functional theory; the structure of such a calculation was given particularly clearly in Ref. 15. Regretably, most,[14,15,30,31,38] but not all,[39] of the density-functional calculations have unwittingly used a nonstandard definition of $\zeta$, herein called $\zeta'$. The value $\zeta'=0$ is the same as $\zeta=0$; however, $\zeta'=1$ corresponds to the situation in which the [111] bond length remains constant under distortion, i.e., $\frac{3}{2}\zeta'=\zeta$ (Ref. 14). The values of the theory presented in Table IV include the factor $\frac{3}{2}=\zeta/\zeta'$ where appropriate to adjust for the different definitions of $\zeta$. The existence of two definitions for $\zeta$ seems not to have been noticed before; indeed, Christensen[38] demonstrates the necessity of $0.40\leqslant\zeta'\leqslant0.60$ within LAPW, whereas the most recent experimental values are $\zeta=0.72\pm0.02$ and $\zeta=0.74\pm0.02$, and concludes there is an inconsistency. Converting $\zeta'$ to $\zeta$, Christiensen's inequality becomes $0.60\leqslant\zeta\leqslant0.90$ which is well satisfied by the experiments. Similarly, Wei, Allan, and Wilkins[31] argue in a footnote that the experimental values violate $\zeta'\leqslant\frac{2}{3}$ (or, equivalently, $\zeta\leqslant1$), but their argument is flawed because of confusion over conventions: $\zeta'\leqslant\frac{2}{3}$ and $\zeta\leqslant1$ are required, but $\zeta\leqslant\frac{2}{3}$ is not. The experiments always report $\zeta$ not $\zeta'$, and the actual values (0.72 or 0.74) given above are less than 1. As seen in Table IV, there is in fact a reasonable agreement among the two most recent experiments and all of the theory except the two earliest calculations. Table IV suggests that $\zeta$ is predictable with an accuracy of about 0.1 unit or 10% of its *a priori* allowed range.[36]

In the fluorite structure (which includes most of the materials in this study), the fluorine anions occupy a simple

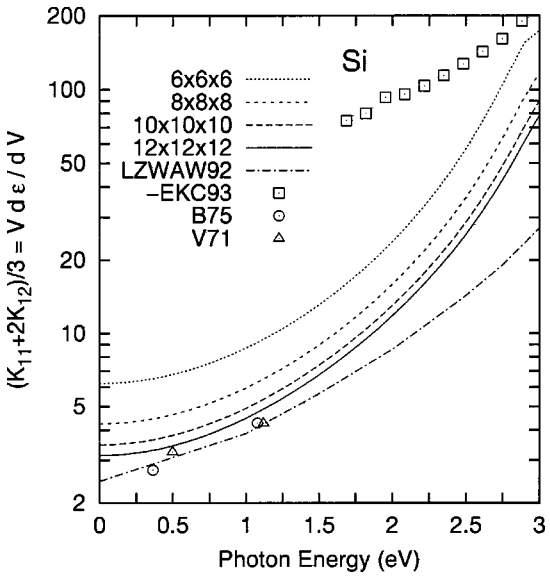


FIG. 1. Hydrostatic photoelastic constant $(K_{11}+2K_{12})/3 = V\,d\epsilon/dV$ for Si, including theory for various values of the full Brillouin zone sampling grid, the previous theory (density-functional pseudopotential calculation using plane waves and a scissors operator to correct the self-energy) of Ref. 14 (LZWAW92), and the previous experiments Refs. 41 (V71), 42 (B75), and 44 (−EKC93) (which appears with its sign switched).

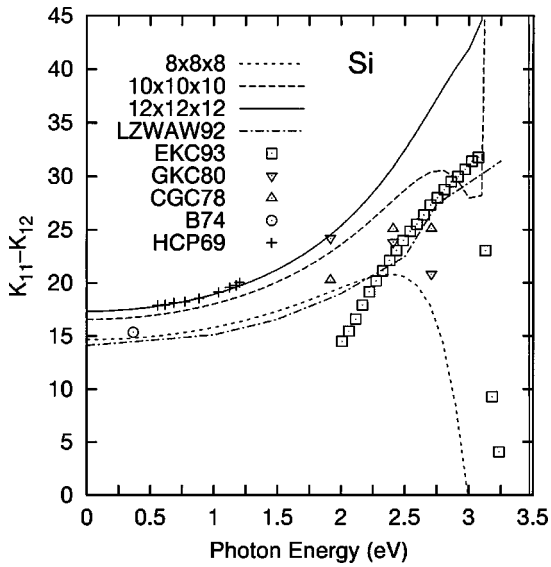


FIG. 2. Photoelastic constant $K_{11}-K_{12}$ ([001] strain) for Si, including theory for various values of the full Brillouin zone sampling grid, previous theory Ref. 14 (LZWAW92), and the previous experiments of Refs. 43 (HCP69), 51 (B74), 52 (CGC78), 53 (GKC80), and 44 (EKC93). Note the part of the $12\times12\times12$ curve at the extreme right in the figure.

cubic lattice; the cations are located at the centers of alternate cubes in a face-centered-cubic lattice. The lattice responds as the diamond lattice does to strain: with [111] strain the fluorine atoms are free to move symmetrically about the cation along the [111] line; if the cation is ignored, the definition of $\zeta$ given for the diamond lattice may be used for the fluorite structure as well. Similarly, there are no internal degrees of freedom under hydrostatic strain or $[1\bar{1}0]$ strain. The only previous work on the internal strain parameter in the fluorite structure solids of which we are aware is a force-field model due to Sharma and Goyal.[40] As seen in Table IV, these values give the same trend as the present calculation, albeit with lower values.

LiF has the sodium chloride structure which does not have any internal degrees of freedom under strain.

## VI. PHOTOELASTIC PROPERTIES

Silicon is considered first to make contact with its large literature. The results of the calculation for hydrostatic strain are shown in Fig. 1, which includes a convergence study, as well as a comparison to the literature. Numerical convergence with respect to sampling of the Brillouin zone has been achieved to about 15% over the range of 0–2 eV. The Brillouin zone convergence is the largest numerical error in the study. Agreement with earlier experiments (Refs. 41 and 42) at low frequencies is quite good. Agreement with the previous theory[14] based on the local-density approximation with a simple self-energy correction in the form of a ''scissors operator'' is also reasonable, although the deviations become more marked at higher frequencies. The treatment of excitons is explicit in the present work, in contrast to the earlier study, and larger deviations between the theories at higher frequencies are expected. The comparison with the experiment past the indirect gap is obscured because of the neglect of indirect transitions in the present calculation.

The case of uniaxial strain along [001] is shown in Fig. 2. Here the new calculation is in excellent agreement with the low-frequency results of Ref. 43 and gives a fair account of the other experimental data. In particular, the extreme reversal in the data of Ref. 44 above 3 eV is mimicked by the calculation at a slightly higher frequency for the $12\times12\times12$ case. Because numerical convergence could not be achieved so close to the direct gap frequency, the exact numerical prediction is not necessarily representative of the full theory.

The results for uniaxial strain along [111] are shown in Fig. 3. As demonstrated earlier,[14] the results are sensitive to the value of the internal strain parameter $\zeta$ discussed earlier. The present theory is presented with values given by LDA total energy minimization ($\zeta=0.81$) and by comparison with experiment[45,46] ($\zeta=0.73$); see also Table IV. Like the hydrostatic case, the present calculation shows greater variability near the band edges—in this case resolving some of the discrepancy with experiment. Again, the existence of phonon-assisted transitions between the indirect and direct gaps makes comparison to experiment difficult.

LiF, in the rocksalt structure, is the simplest of the fluoride compounds. Theoretical results for the photoelastic tensor under hydrostatic strain are shown in Fig. 4; we are not aware of any comparable experimental results. The case of uniaxial [001] strain is presented in Fig. 5. The theory obtains the correct trends as the data, but disperses too strongly and overestimates the value of $K_{11}-K_{12}$ for all photon energies. In contrast, for the case of uniaxial [111] strain, the

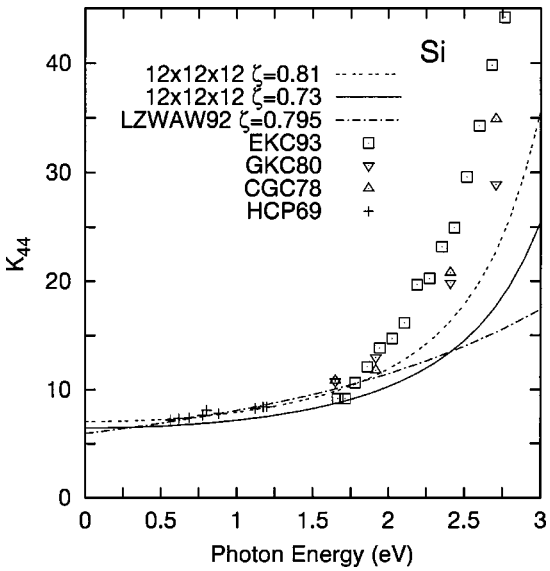


FIG. 3. Photoelastic constant $K_{44}$ ([111] strain) for Si, including theory for two values of the internal strain parameter, $\zeta=0.81$, predicted by our minimization of the total energy, and $\zeta=0.73$, which is representative of the experimental data presented in Table IV. The previous theory of Ref. 14 (LZWAW92) and the previous experiments of Refs. 43 (HCP69), 52 (CGC78), 53 (GKC80), and 44 (EKC93) are also shown.

agreement with experiment is excellent. The predictive power of the theory is to be judged by the worse of these two results—i.e., factor-of-2 agreement with correct trends. Convergence to about 15% or better is achieved by the $8\times8\times8$ sampling grid in all cases (see Fig. 6).

Results for hydrostatic strain for the homologous series $CaF_2$, $SrF_2$, and $BaF_2$ are given in Figs. 7, 8, and 9. At low photon energy, the theory agrees with the available experimental data at a level comparable to the range of experimental values. The dramatic feature predicted at high energy in Figs. 8 and 9 also holds for the case of $CaF_2$, albeit between 10.1 and 10.4 eV. Because this feature is similar to the experimental and theoretical results for silicon shown in Fig. 1, we believe it is real.

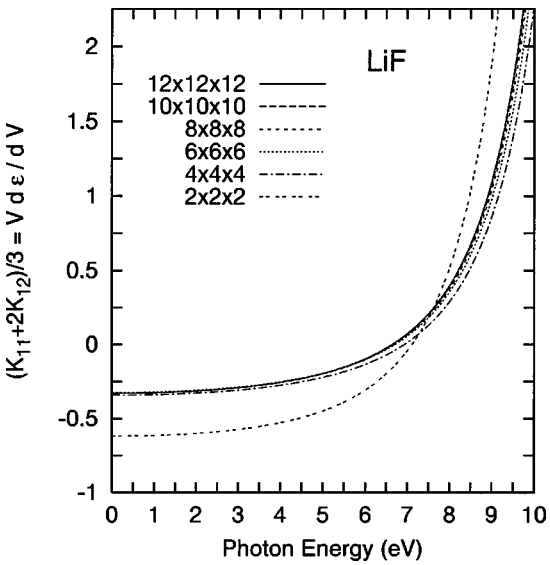


FIG. 4. Hydrostatic photoelastic constant $(K_{11}+2K_{12})/3 = V\,d\epsilon/dV$ for LiF, including theory for various values of the full Brillouin zone sampling grid.

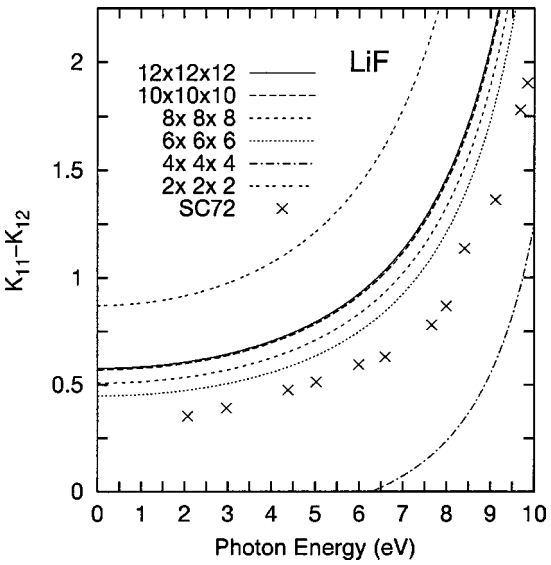


FIG. 5. Photoelastic constant $K_{11}-K_{12}$ ([001] strain) for LiF, including theory for various values of the full Brillouin zone sampling grid. The previous experiment of Ref. 47 (SC72) is also shown.

The results for uniaxial [001] strain are given in Figs. 10, 11, and 12. Like the case of silicon, the magnitude is overestimated compared with experiment, and the dramatic turnaround near 9 eV in the case of $CaF_2$ occurs both in theory and experiment. The measurements of the present work is

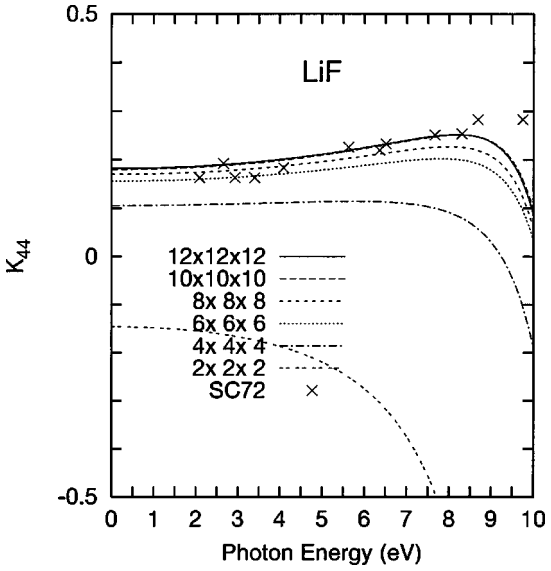


FIG. 6. Photoelastic constant $K_{44}$ ([111] strain) for LiF, including theory for various values of the full Brillouin zone sampling grid. The symmetry of the LiF does not lead to an internal strain parameter under compression in this direction. The previous experiment of Ref. 47 (SC72) is also shown.

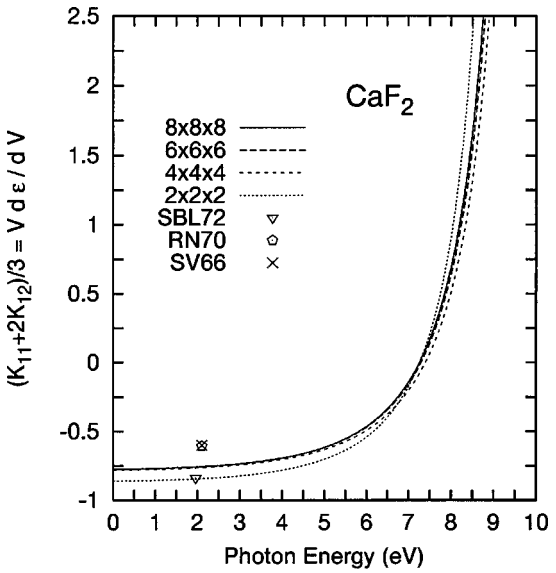


FIG. 7. Hydrostatic photoelastic constant $(K_{11}+2K_{12})/3 = V\,d\epsilon/dV$ for $CaF_2$, including theory for various values of the full Brillouin zone sampling grid and the previous experiments Refs. 54 (SV66), 55 (RN70), and 56 (SBL72).

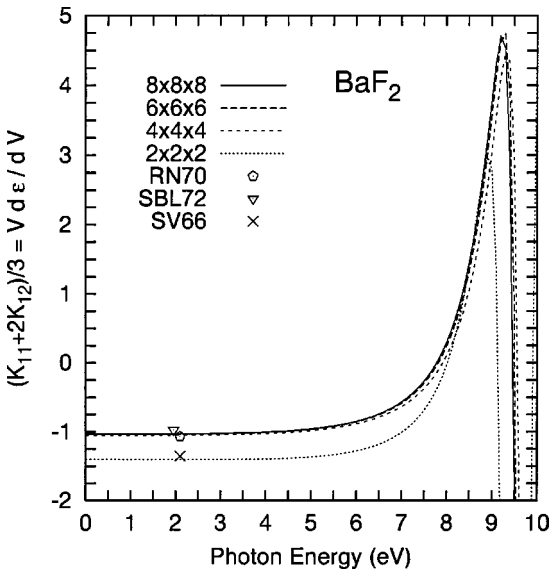


FIG. 9. Hydrostatic photoelastic constant $(K_{11}+2K_{12})/3 = V\,d\epsilon/dV$ for $BaF_2$, including theory for various values of the full Brillouin zone sampling grid and the previous experiments of Refs. 54 (SV66), 55 (RN70), and 56 (SBL72).

consistent with the low-energy measurements of Ref. 48. The origin of the discrepancy between these measurements and Ref. 47 for the case of $SrF_2$ is unclear. The theory, present experiment, and Ref. 48 find the low-frequency values for the series $CaF_2$, $SrF_2$, and $BaF_2$ to be roughly constant on the scale of the factor-of-3 difference reported by Ref. 47 for $SrF_2$ only.

The results for uniaxial [111] strain are given in Figs. 13, 14, and 15 for $CaF_2$, $SrF_2$, and $BaF_2$, respectively. As noted by Sánchez and Cardona[47] and seen the measurements of the present work, for both the [001] and [111] cases, the dispersion of $SrF_2$ is intermediate between $CaF_2$ and $BaF_2$. It is interesting to note that the same relationship holds for the dispersion of the intrinsic birefringence.[3,49]

As noted earlier for the case of silicon in Ref. 14 and Fig. 3, the photoelastic tensor component $K_{44}$ is a sensitive function of the internal strain parameter $\zeta$. Moreover, the internal strain parameter is not known experimentally for the fluorides. Hence we take two approaches. As discussed earlier and presented in Table IV, a total-energy LDA minimization was performed yielding theoretical values for $\zeta$. The results for the photoelastic tensor component $K_{44}$ using this proce-

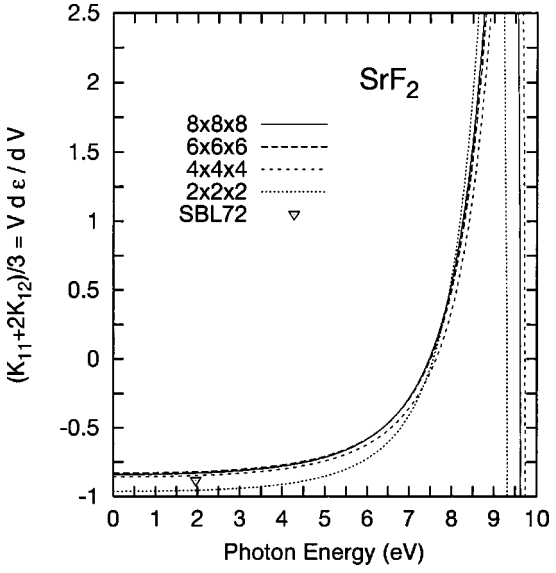


FIG. 8. Hydrostatic photoelastic constant $(K_{11}+2K_{12})/3 = V\,d\epsilon/dV$ for $SrF_2$, including theory for various values of the full Brillouin zone sampling grid and the previous experiment Ref. 56 (SBL72).

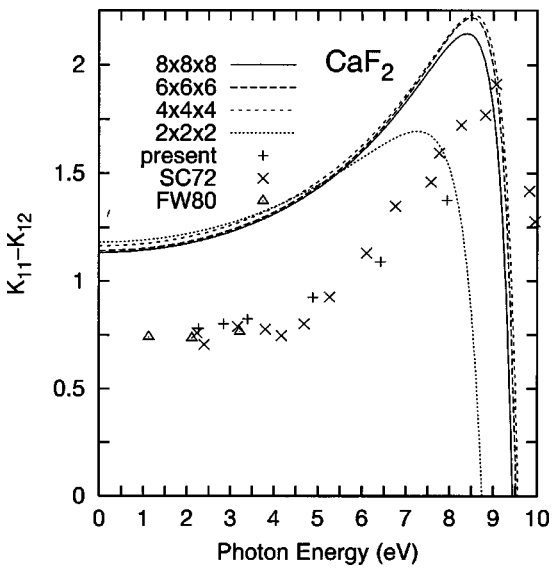


FIG. 10. Photoelastic constant $K_{11}-K_{12}$ ([001] strain) for $CaF_2$, including theory for various values of the full Brillouin zone sampling grid, the present experiment, and the previous experiments of Refs. 47 (SC72) and 48 (FW80).

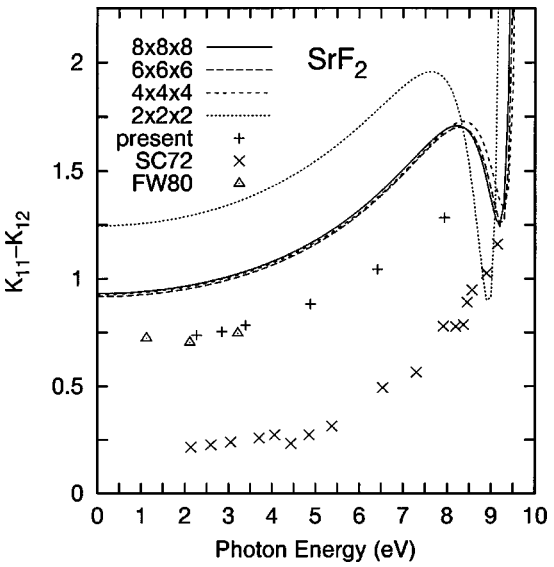


FIG. 11. Photoelastic constant $K_{11}-K_{12}$ ([001] strain) for $SrF_2$, including theory for various values of the full Brillouin zone sampling grid, the present experiment, and the previous experiments of Refs. 47 (SC72) and 48 (FW80).

dure are in excellent agreement with experiment for the case of $CaF_2$, but not for $SrF_2$ and $BaF_2$. Hence we also regard $\zeta$ as a fitting parameter. As shown in Figs. 14 and 15, a good account of the data may be obtained with a change in $\zeta$ of 0.2–0.3. Given the paucity of experience in fitting $\zeta$ to experiment (Si being the only case known to us), it is difficult to estimate the uncertainty in the theoretical estimate of $\zeta$ for the fluorides, so it is possible to ascribe the difference in the theoretical prediction and experiment to a lack of knowledge of $\zeta$. On the other hand, the theoretical overestimate of $K_{11}-K_{12}$ (which is independent of $\zeta$) leads us to lack full confidence in this fitting procedure. The best that can be said is that both the low-frequency data and the sign of the dispersion are accounted for semiquantitatively if $\zeta$ is taken as a fitting parameter.

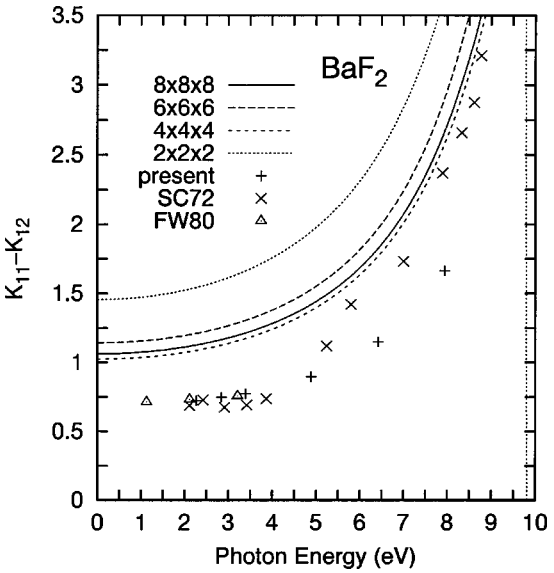


FIG. 12. Photoelastic constant $K_{11}-K_{12}$ ([001] strain) for $BaF_2$, including theory for various values of the full Brillouin zone sampling grid, present measurements (+), and the previous experiments of Refs. 47 (SC72) and 48 (FW80).

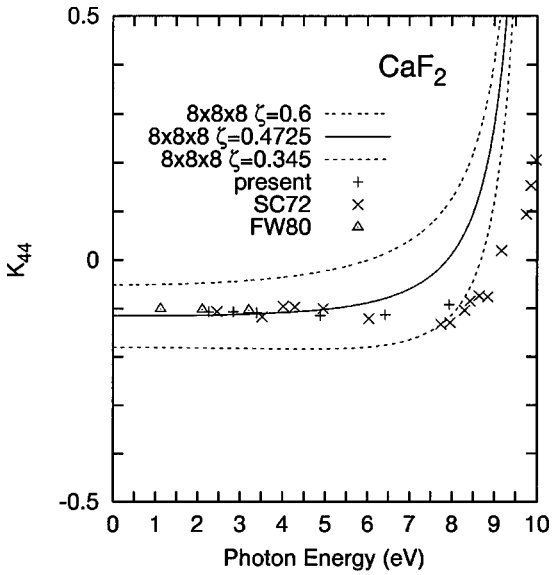


FIG. 13. Photoelastic constant $K_{44}$ ([111] strain) for $CaF_2$, including theory for various values of the full Brillouin zone sampling grid at $\zeta=0.4725$, determined by LDA total-energy minimization, and various values of the sampling grid, the present experiment, and the previous experiments of Refs. 47 (SC72) and 48 (FW80).

It is very difficult to achieve numerical convergence of the photoelastic tensor close to the band edge. The low-frequency results are more reliable than their higher-frequency counterparts. Nevertheless, the predictions near the band edge—in particular the prediction of a single dra-

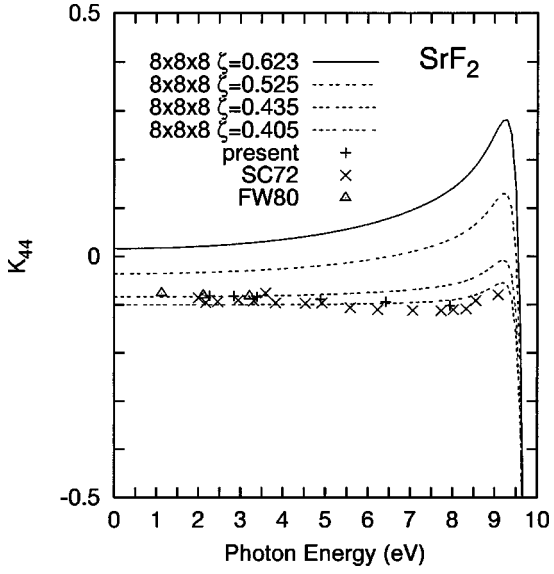


FIG. 14. Photoelastic constant $K_{44}$ ([111] strain) for $SrF_2$, including theory for various values of the full Brillouin zone sampling grid at $\zeta=0.623$ and various values of the internal strain parameter $\zeta$ for the $8\times8\times8$ sampling grid, the present experiment, and the previous experiments of Refs. 47 (SC72) and 48 (FW80).

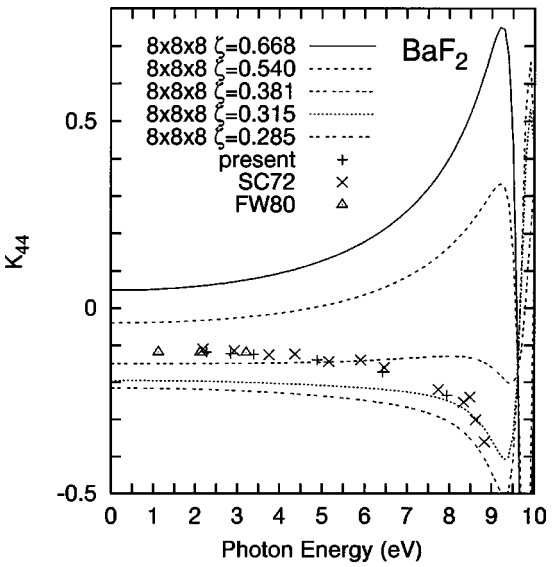


FIG. 15. Photoelastic constant $K_{44}$ ([111] strain) for $BaF_2$, including theory for various values of the internal strain parameter $\zeta$, present measurements (+), and the previous experiments of Refs. 47 (SC72) and 48 (FW80).

matic turnover in many cases—correctly describe the trends in the data. Similar agreement for the sign and qualitative dispersion of $CaF_2$, $SrF_2$, and $BaF_2$ for the intrinsic birefringence was observed previously.[3] The case of the hydrostatic strain in silicon (see Fig. 1) is troubling, however, and should perhaps be rechecked experimentally with a single set of measurements across the indirect band gap.

Given the potential technological importance of mixed crystals $Ca_xSr_{1-x}F_2$ for 157 nm lithography, we have calculated the three photoelastic tensor components for these materials for three values of $x$ in the virtual-crystal approximation in addition to the pure materials. The results are shown in Figs. 16, 17, and 18. For uniaxial [111] strain, $\zeta$ is linearly interpolated between the best-fit values obtained for the pure materials. The photoelastic tensor components are predicted to have a richer structure than merely interpolating linearly between the end points of the two pure materials.

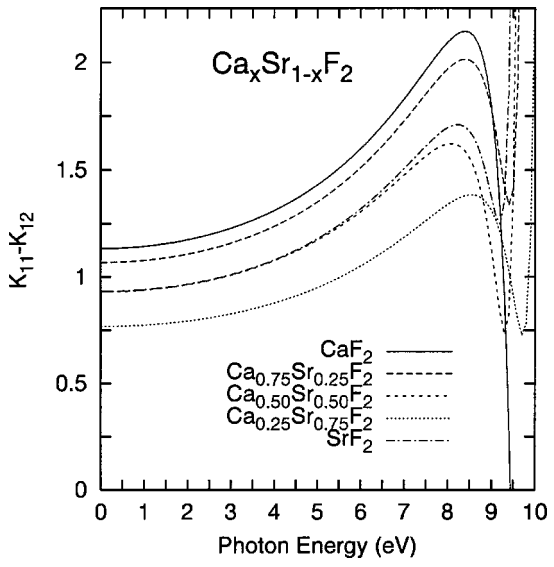


FIG. 17. Photoelastic constant $K_{11}-K_{12}$ ([001] strain) for $Ca_xSr_{1-x}F_2$ with parameters as in Fig. 16.

## VII. CONCLUSIONS

The elastic moduli and photoelastic tensors have been calculated for Si, LiF, $CaF_2$, $SrF_2$, $BaF_2$, and $Ca_xSr_{1-x}F_2$ and compared to experimental results from the literature as well as to new measurements of the photoelastic tensors for

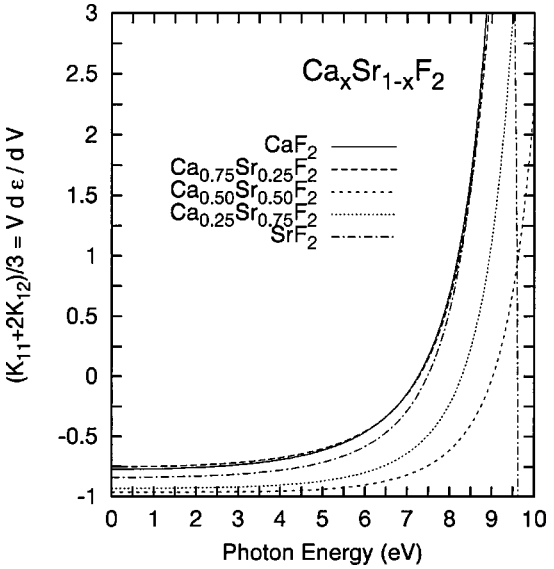


FIG. 16. Hydrostatic photoelastic constant $(K_{11}+2K_{12})/3 = V\,d\epsilon/dV$ for $Ca_xSr_{1-x}F_2$, $x=0$, 0.25, 0.50, 0.75, 1, for the full Brillouin zone sampling grid of $8\times8\times8$ with the lattice constant interpolated between the experimental values of $CaF_2$ and $SrF_2$.

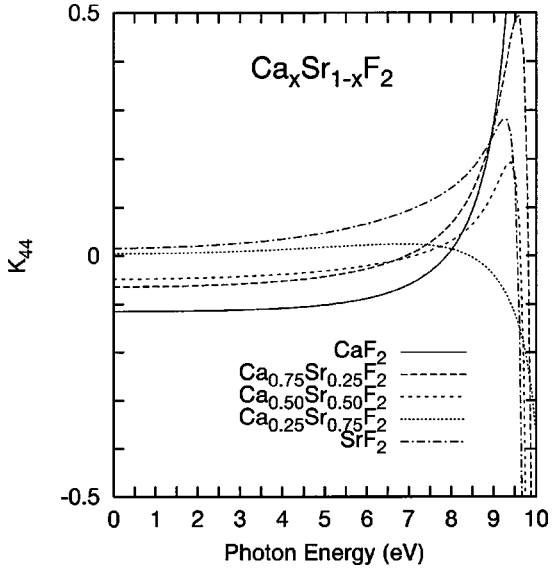


FIG. 18. Photoelastic constant $K_{44}$ ([111] strain) for $Ca_xSr_{1-x}F_2$, with parameters as in Fig. 16. The internal strain parameter $\zeta$ is interpolated between 0.473 and 0.404, the best-fit values for $CaF_2$ and $SrF_2$, respectively.

$CaF_2$, $SrF_2$, and $BaF_2$. The calculations have been performed including excitonic effects via the Bethe-Salpeter equation for the photoelastic properties; for the elastic moduli, the local-density approximation is used. The elastic moduli have been found not only for their own sake, but to determine the internal strain parameter $\zeta$, which is required to predict the photoelastic property under [111] uniaxial strain.

Typically, a factor-of-2 agreement with experiment is obtained for the photoelastic properties, with the dispersion reasonably given. However, some of the experiments in the literature are in contradiction with each other. In particular, the present measurements and theory support the value of Ref. 48 over that of Ref. 47 for the photoelastic tensor of $SrF_2$ associated with [001] strain.

Each example of strain-induced birefringence has a static value and varies rapidly in some fashion as a band edge or exciton peak is approached. Such rapid variation is greatly enhanced in wide-gap insulators by the presence of excitonic peaks, as may be deduced from Kramers-Kronig arguments. Local-field effects of the $K_{xc}$ of density-functional calculations are known not to produce excitonic peaks. We may therefore credit the inclusion of excitonic effects with the functional form of the birefringence at higher energies in the wide-gap insulators. This is not as clear for semiconductors, however, in part because of difficulties with the existence of the indirect band gap in silicon and with difficulties of *k*-point convergence previously demonstrated in the case of GaAs.[50]

We believe that the apparent inability of the local-density approximation to account for the internal strain parameter $\zeta$ of silicon was merely because of the existence of two contradictory definitions for $\zeta$ which were unwittingly confused. That is, given consistent definitions, our calculation and earlier calculations are in agreement with x-ray diffraction experiments to better than 0.1 for $\zeta$ (whose full physical range[36] is 1).

The results given here may be of importance to the semiconductor lithography community because of the potential application of calcium fluoride and related materials to lithography based on ultraviolet light of 193 and 157 nm.

## ACKNOWLEDGMENTS

The authors acknowledge useful discussions with Douglas C. Allan and support for the computation from Eite Tiesinga. Funding for the experimental program was provided in part by SEMATECH.

[1] G. E. Moore, Electronics **38**, 8 (1965).
[2] Semiconductor Industry Association, *International Technology Roadmap for Semiconductors* (SEMATECH, San Jose, CA, 2001), Interconnect Chapter, p. 5; http://public.itrs.net/Files/2001ITRS/Home.htm.
[3] J. H. Burnett, Z. H. Levine, and E. L. Shirley, Phys. Rev. B **64**, 241102 (2001).
[4] J. H. Burnett, Z. H. Levine, E. L. Shirley, and J. Bruning, J. Microlithogr. Microfabrication Microsyst. **1**, 213 (2002).
[5] B. Wang, Solid State Technol. **43**, 77 (2000).
[6] E. Chernevskaya and G. Ananéva, Sov. Phys. Solid State **8**, 169 (1966).
[7] L. M. Iomin and A. I. Livshits, J. Struct. Chem. **35**, 265 (1994).
[8] J. H. Burnett, Z. H. Levine, and E. L. Shirley, *Minimizing spatial-dispersion-induced birefringence in crystals used for precision optics by using mixed crystals of materials with the opposite sign of the birefringence* (NIST, Gaithersburg, MD, 2001), physics.nist.gov/Divisions/Div842/Gp3/DUVMatChar/birefring.html; also U.S. patent pending.
[9] H. J. McSkimin, J. Appl. Phys. **24**, 988 (1953).
[10] C. V. Briscoe and C. V. Squire, Phys. Rev. **106**, 1175 (1957).
[11] P. S. Ho and A. L. Ruoff, Phys. Rev. **161**, 864 (1967).
[12] D. Gerlich, Phys. Rev. **135**, A1331 (1964).
[13] D. Gerlich, Phys. Rev. **136**, A1366 (1964).
[14] Z. H. Levine, H. Zhong, S. Wei, D. C. Allan, and J. W. Wilkins, Phys. Rev. B **45**, 4131 (1992).
[15] J. Sánchez-Dehesa, C. Tejedor, and J. A. Vergés, Phys. Rev. B **26**, 5960 (1982).
[16] D. R. Hamann, M. Schlüter, and C. Chiang, Phys. Rev. Lett. **43**, 1494 (1979).
[17] D. Vanderbilt, Phys. Rev. B **32**, 8412 (1985).
[18] E. L. Shirley, X. J. Zhu, and S. G. Louie, Phys. Rev. B **56**, 6648 (1997).
[19] Z. H. Levine and D. C. Allan, Phys. Rev. B **44**, 12 781 (1991); **48**, 14 768(E) (1993).
[20] D. M. Ceperley and B. J. Alder, Phys. Rev. Lett. **45**, 566 (1980).
[21] J. P. Perdew and A. Zunger, Phys. Rev. B **23**, 5048 (1981).
[22] E. L. Shirley, L. J. Terminello, J. E. Klepeis, and F. J. Himpsel, Phys. Rev. B **53**, 10 296 (1996).
[23] L. X. Benedict and E. L. Shirley, Phys. Rev. B **59**, 5441 (1999).
[24] Z. H. Levine and D. C. Allan, Phys. Rev. B **43**, 4187 (1991).
[25] E. L. Shirley, Phys. Rev. B **58**, 9579 (1998).
[26] Z. H. Levine and S. G. Louie, Phys. Rev. B **25**, 6310 (1982).
[27] M. S. Hybertsen and S. G. Louie, Phys. Rev. B **37**, 2733 (1988).
[28] A. Feldman, Opt. Eng. (Bellingham) **17**, 453 (1978).
[29] A. Feldman and W. J. McKean, Rev. Sci. Instrum. **46**, 1588 (1975).
[30] O. H. Nielsen and R. M. Martin, Phys. Rev. B **32**, 3792 (1985).
[31] S. Wei, D. C. Allan, and J. W. Wilkins, Phys. Rev. B **46**, 12 411 (1992).
[32] W. Hayes and A. M. Stoneham, in *Crystals with the Fluorite Structure*, edited by W. Hayes (Clarendon, Oxford, 1974), p. 47.
[33] P. Cortona, Phys. Rev. B **46**, 2008 (1992).
[34] M. Mérawa, M. Llunell, R. Orlando, M. Gelize-Duvnau, and R. Dovesi, Chem. Phys. Lett. **368**, 7 (2003).
[35] A. D. Becke, J. Chem. Phys. **98**, 5648 (1993).
[36] L. Kleinman, Phys. Rev. **128**, 2614 (1962).
[37] C. S. G. Cousins, J. Phys. C **15**, 1857 (1982).
[38] N. E. Christensen, Solid State Commun. **50**, 177 (1984).
[39] B. N. Harmon, W. Weber, and D. R. Hamann, Phys. Rev. B **25**, 1109 (1982).

[40] A. K. Sharma and S. C. Goyal, Phys. Status Solidi B **157**, 145 (1990).
[41] R. Vetter, Phys. Status Solidi A **8**, 443 (1971).
[42] D. K. Biegelsen, Phys. Rev. B **12**, 2427 (1975).
[43] C. W. Higginbotham, M. Cardona, and F. H. Pollak, Phys. Rev. **184**, 821 (1969).
[44] P. Etchegoin, J. Kircher, and M. Cardona, Phys. Rev. B **47**, 10 292 (1993).
[45] C. S. G. Cousins, L. Gerward, J. S. Olsen, B. Selsmark, and B. J. Sheldon, J. Appl. Crystallogr. **15**, 155 (1982).
[46] H. d'Amour, W. Denner, H. Schulz, and M. Cardona, J. Appl. Crystallogr. **15**, 148 (1982).
[47] C. Sánchez and M. Cardona, Phys. Status Solidi B **50**, 293 (1972).
[48] A. Feldman and R. M. Waxler, Phys. Rev. Lett. **45**, 126 (1980).
[49] J. H. Burnett, E. L. Shirley, and Z. H. Levine (unpublished).
[50] J. E. Raynolds, Z. H. Levine, and J. W. Wilkins, Phys. Rev. B **51**, 10 287 (1995).
[51] D. K. Biegelsen, Phys. Rev. Lett. **32**, 1196 (1974).
[52] M. Chandrasekhar, M. H. Grimsditch, and M. Cardona, Phys. Rev. B **18**, 4301 (1978).
[53] M. H. Grimsditch, E. Kisela, and M. Cardona, Phys. Status Solidi A **60**, 135 (1980).
[54] E. D. D. Schmidt and K. Vedam, J. Phys. Chem. Solids **27**, 1563 (1966).
[55] K. V. Rao and T. S. Narasimhamurty, J. Phys. Chem. Solids **31**, 876 (1970).
[56] O. V. Shakin, M. F. Bryzhina, and V. V. Lemanov, Sov. Phys. Solid State **13**, 3141 (1972).
[57] H. J. Monkhorst and J. D. Pack, Phys. Rev. B **13**, 5188 (1976).
[58] L. Vegard, Z. Phys. **5**, 17 (1921).
[59] D. F. Bezuidenhout, in *Handbook of Optical Constants of Solids II*, edited by E. D. Palik (Academic, New York, 1998), p. 815ff.
[60] R. Gupta, J. H. Burnett, U. Griesmann, and M. Walhout, Appl. Opt. **37**, 5964 (1998).
[61] J. H. Burnett, R. Gupta, and U. Griesmann, Appl. Opt. **41**, 2508 (2002).
[62] M. E. Thomas and W. J. Tropf, in *Handbook of Optical Constants of Solids III*, edited by E. D. Palik (Academic, New York, 1998), p. 683ff.
[63] A. Segmüller, Phys. Kondens. Mater. **3**, 18 (1964).
[64] A. Segmüller and H. R. Neyer, Phys. Kondens. Mater. **4**, 63 (1965).